



# Atmospheric response to seasonal changes in sea surface temperature during the boreal summer in the Tropical Atlantic

Dahirou Wane, Gaëlle de Coëtlogon, Alban Lazar, Malick Wade, Amadou T Gaye

## ► To cite this version:

Dahirou Wane, Gaëlle de Coëtlogon, Alban Lazar, Malick Wade, Amadou T Gaye. Atmospheric response to seasonal changes in sea surface temperature during the boreal summer in the Tropical Atlantic. *Climate Dynamics*, 2024, 62 (3), pp.1597 - 1612. 10.1007/s00382-023-06968-4. insu-04288175v1

**HAL Id: insu-04288175**

**<https://insu.hal.science/insu-04288175v1>**

Submitted on 15 Nov 2023 (v1), last revised 28 Feb 2024 (v2)

**HAL** is a multi-disciplinary open access archive for the deposit and dissemination of scientific research documents, whether they are published or not. The documents may come from teaching and research institutions in France or abroad, or from public or private research centers.

L'archive ouverte pluridisciplinaire **HAL**, est destinée au dépôt et à la diffusion de documents scientifiques de niveau recherche, publiés ou non, émanant des établissements d'enseignement et de recherche français ou étrangers, des laboratoires publics ou privés.



# Atmospheric response to seasonal changes in sea surface temperature during the boreal summer in the Tropical Atlantic

Dahirou Wane<sup>1</sup> · Gaëlle de Coëtlogon<sup>2</sup> · Alban Lazar<sup>3</sup> · Malick Wade<sup>4</sup> · Amadou T. Gaye<sup>1</sup>

Received: 23 September 2022 / Accepted: 20 September 2023  
© The Author(s) 2023

## Abstract

We investigate the atmospheric response to seasonal variations in sea surface temperature (SST) in the eastern tropical Atlantic during the boreal summer, using the Weather Research and Forecasting (WRF) regional atmospheric model. Three ensembles of 11 simulations each are produced with different SST forcings: the control ensemble (CTL) uses the observed climatology of the SST in 2000–2009, while the Frozen North (FzN) and Frozen South (FzS) experiments block the seasonal warming or cooling of the SST from June onwards in a region confined to the eastern tropical Atlantic. The result is a cold SST anomaly in the northeastern tropical Atlantic off the coasts of Senegal and Mauritania in FzN, and a warm anomaly in the southeastern region (Gulf of Guinea and the cold tongue zone in the equatorial Atlantic) in FzS. Comparison with CTL reveals significant impacts of these SST anomalies on the position and intensity of the marine intertropical convergence zone (ITCZ) and on West African rainfall during July and August. Over the ocean, the cold anomaly in NETA suppresses convection on the northern side of the ITCZ (north of 10°N), while the warm anomaly in the Gulf of Guinea strengthens convection on its southern flank. The latter is also leading to a sharp increase in precipitation in the coastal regions to the northeast of the Gulf of Guinea. These changes are clearly due to variations in surface pressure gradients and the divergence of low-level moisture in response to SST anomalies, which in turn induce changes in deep atmospheric convection through thermodynamic feedback. On the continent, a substantial reduction in precipitation is observed in the western Sahel (particularly Senegal) following the cold anomaly in NETA, and in the eastern Sahel following the warm anomaly in the Gulf of Guinea: both are explained by a positive anomaly in the divergence of moisture transport in the upper troposphere, associated with an acceleration of the African easterly jet along its southern edge. However, the mechanism by which the SST anomalies create this acceleration in both experiments remains to be elucidated.

**Keywords** Tropical Atlantic · Intertropical Convergence Zone · Weather and Research Forecast regional atmospheric model · Sensitivity experiments · West African Monsoon · Air-sea interaction

✉ Dahirou Wane  
wane.dahirou@esp.sn; mahasimw@gmail.com

Gaëlle de Coëtlogon  
gaelle.decoetlogon@latmos.ipsl.fr

Alban Lazar  
alban.lazar@locean-ipsl.upmc.fr

Malick Wade  
malick.wade@ugb.edu.sn

Amadou T. Gaye  
atgaye@ucad.edu.sn

<sup>1</sup> Laboratoire de Physique de l'Atmosphère et de l'Océan Siméon Fongang (LPAO-SF/ESP/UCAD), Dakar 10200, Senegal

<sup>2</sup> Laboratoire atmosphères, milieux, observations spatiales (LATMOS/UPMC/SU), 75252 Paris, France

<sup>3</sup> Laboratoire d'Océanographie et du Climat: Expérimentations et Approches Numériques (LOCEAN/UPMC/SU), 75252 Paris, France

<sup>4</sup> Laboratoire des Sciences de l'Atmosphère et des Océans (LSAO/UGB), Saint-Louis 234, Senegal

# 1 Introduction

The tropical Atlantic region encompasses a variety of coupled climate variations that significantly impact continental precipitation, hurricane activity in the Atlantic, ocean-based biological productivity and atmospheric circulation in the equatorial Pacific (Foltz et al. 2019). However, climate models currently struggle to accurately represent this region. Wahl et al. (2011) demonstrated that the prevalent warm bias found in the southeastern Tropical Atlantic sea surface temperature (SST) in a climate model leads to major challenges in simulating present and future climate, particularly precipitation. In addition, the SST in the Eastern Tropical Atlantic plays an important role in representing and predicting the African Monsoon on seasonal and decadal timescales (Hulme et al. 2001). Due to its significant impact on the quality of life of surrounding populations, understanding the influence of SST in the Eastern Tropical Atlantic on West African rainfall variability is crucial.

The region exhibits a pronounced seasonal cycle of SST, surface wind, and convective activity (Mitchell and Wallace 1992; Li and Philander 1997; Gu and Adler 2004; Richter et al. 2017; Rugg et al. 2016). The InterTropical Convergence Zone (ITCZ), where the Trade Winds

converge, migrates from the Equator during boreal winter months to approximately 10°N during boreal summer months (Fig. 1, top). Wane et al. (2021) defined the Atlantic Warm Pool as the region associated with the Atlantic ITCZ, characterized by heavy precipitation and converging surface winds. The position and intensity of the ITCZ are partly determined by the SST, with warm SSTs favoring deep convection and convergence of surface winds (Waliser and Graham 1993; Lin et al. 2006; Gill 1980). The climatological seasonal cycle of the ITCZ position involves multiple processes, including SST-induced adjustments in the atmospheric boundary layer, such as changes in surface pressure and convergence in the lower layers (Biasutti et al. 2004). The importance of the SST in the eastern tropical Atlantic, particularly the Atlantic Cold Tongue (ACT) SST, in the northward displacement of the ITCZ and associated precipitation intensity, has been well-established: numerous studies have emphasized the role of SST in the tropical Atlantic Ocean on the climate of surrounding continents, particularly West Africa (Sultan and Janicot 2003; Gu and Adler 2004; Okumura and Xie 2004; Brandt et al. 2011; Meynadier et al. 2016; Crespo et al. 2019). For example, Crespo et al. (2019) demonstrated the strong influence of the seasonal evolution of the West African monsoon and ITCZ by the seasonal variations of ACT SST. Similarly, Okumura and Xie (2004) highlighted

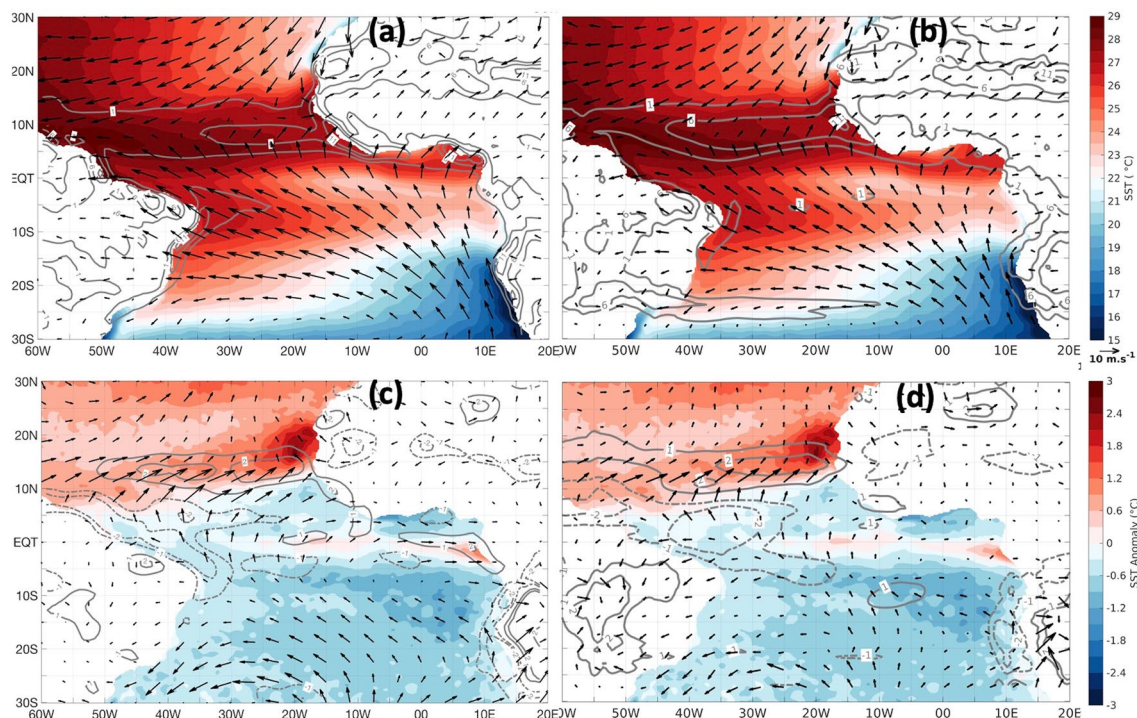


**Fig. 1** 2000–2009 SST (in °C, Reynolds product, shading), 10 m-wind divergence (in  $10^{-5} \text{ s}^{-1}$ , contours), and 10 m-wind (in m/s, vectors) in the July–August average (**a**, **b**) and the difference between

August and July (**c**, **d**). The surface wind and convergence in (**a**) and (**c**) are derived from ERAI reanalyses, while those in (**b**) and (**d**) are obtained from the control simulation (CTL)

the significance of the cooling of ACT SST in spring on the northward migration of the ITCZ for the West African Monsoon. The meridional migration of the ITCZ from July to August plays a crucial role in rainfall patterns across West Africa and northern South America (Tomaziello et al. 2016; Sultan and Janicot 2000, 2003; Giannini et al. 2005; Hastenrath 2006; Hounsou-Gbo et al. 2015).

The interactions between SST and surface winds in the equatorial band occur on short timescales due to the rapid dynamical response of the atmosphere and ocean (de Coëtlogon et al. 2010). The SST mainly affects the wind through local modifications of the pressure gradient and influences the large-scale pressure gradient controlled by the free troposphere above the marine atmospheric boundary layer (Lindzen and Nigam 1987). The pressure adjustment mechanism was shown to be the main driver of the surface wind convergence in the eastern Tropical Atlantic and Gulf of Guinea (Crespo et al. 2019; de Coëtlogon et al. 2014).

On a seasonal scale, West African rainfall is conditioned by the evolution of the ITCZ (Sultan and Janicot 2003; Gu and Adler 2004), which is largely influenced by seasonal SST anomalies. Okumura and Xie (2004) show a significant influence of the seasonal cooling of the ACT SST on the West African Monsoon (WAM) via the intensification of the southerly winds in the Gulf of Guinea (GG), which pushes the rain band north of the Gulf; and the WAM remains blocked in the south if the ACT does not develop. Thus, a cooling of the tropical East Atlantic SST in boreal spring and summer is associated with the northward migration of the WAM, while warming in this region leads to a blocking of the rain band in the Guinean regions. Another modeling (Meynadier et al. 2016) or diagnostic (Diakhaté et al. 2018) studies found that meridional gradients of SST are closely related to gradients of SLP and meridional winds in the Gulf of Guinea. These mechanisms strongly impact the humidity transport convergence near the coast, leading to the first rainy season of the WAM system (Leduc-Leballeur et al. 2013; Tanguy et al. 2022).

The role of SST on summer rainfall variability in West Africa has thus been relatively well documented for the Gulf of Guinea (Vizy and Cook 2001; Joly and Voldoire 2010; Steinig et al. 2018), but this is not yet the case for the SST in the northeastern Tropical Atlantic. As these results have the potential to improve the representation of ITCZ and WAM seasonal variability in general circulation models (GCMs), it is important to better understand the ocean–atmosphere interactions, in particular on the role of the seasonal cycle of the northeast Tropical Atlantic SST on WAM seasonal variability. This study builds upon previous research conducted by Wane et al. (2021), which examines the mechanisms that underlie the seasonal meridional migration of the tropical Atlantic warm pool. The latter was carried out using data from the 2000–2009 climatological period, as it aligns with

the availability of ocean simulation data (using the NEMO model configured for the Tropical Atlantic at a resolution of  $0.25^\circ$ ) and observed surface wind data (obtained from the QuikSCAT product). The West African monsoon has been categorized into four main phases: oceanic, coastal, transitional, and Sahelian (Thorncroft et al. 2011). The objective of the current study is to examine the influence of northeastern Tropical Atlantic sea surface temperatures (SST) on the Intertropical Convergence Zone (ITCZ) during the Sahelian phase of precipitation. This investigation utilizes the Weather Research and Forecasting (WRF) model: we examine the difference between the control simulation ensemble and the experimental ones where we eliminated the seasonal progression during July and August, therefore deducing the impact of the resulting SST anomalies on surface parameters (sea level pressure and surface winds) over the ocean, as well as on the transport of humidity and precipitation over the continent. The article presents the datasets and describes the experimental setup in Sect. 3, compares the model results with observations in Sect. 4, highlights the main findings in Sect. 5, and concludes with a summary of the results in Sect. 6.

## 2 Data and methods

### 2.1 Data

The study employs the following monthly climatological averages for the period of 2000–2009, obtained from observational-based and reanalysis products, to force the model and validate its output:

- the European Centre for Medium-Range Weather Forecasts (ECMWF) Interim reanalysis (ERA-Interim, Dee et al. 2011),
- the National Oceanic and Atmospheric Administration (NOAA) Optimal Interpolated Sea Surface Temperature (OISST, Reynolds et al. 2007) dataset,
- the Tropical Rainfall Measuring Mission (TRMM) 3B42, which provides daily data with a horizontal resolution of  $0.25^\circ \times 0.25^\circ$  (Huffman et al. 2007).

### 2.2 Model and experimental design

Numerical simulations were conducted with version 3.9.1 of the Weather for Research and Forecasting (WRF, Samarrock et al. 2008), a regional atmospheric model developed by the National Center for Atmospheric Research (NCAR). The model was run at a horizontal resolution of  $0.25^\circ \times 0.25^\circ$  and consisted of 51 vertical layers (from the surface up to 50 hPa). The simulation domain covered the tropical Atlantic ( $30^\circ\text{S}$ – $35^\circ\text{N}$  and  $60^\circ\text{W}$ – $50^\circ\text{E}$ ). The parameterization schemes



used in this study are detailed in Meynadier et al. (2015). Deep convection was parameterized using Betts, Miller, and Janjic scheme (BMJ, Janjić 1994). Microphysics were represented by the WRF Single-Moment 6-Class (WSM6-Class, Hong and Lim 2006). The planetary boundary layer (PBL) was parameterized using Mellor, Yamada and Janjic (MYJ) scheme (Janjić 1994). Radiation was handled by the Rapid Radiative Transfer Model for General Circulation models (RRTMG) scheme (Iacono et al. 2008). The surface layer scheme employed the Monin-Obukhov scheme.

To distinguish numerical noise in the model from inter-annual variability, 11 simulations were conducted using a climatology of forcing parameters. These parameters were seasonally averaged every 6 h for the period of 2000–2009, rather than running a simulation for each year in the period. Lateral forcing of the model was achieved using a seasonal mean of ECMWF ERA-Interim reanalyses, computed every 6 h from April 1 to August 31 over the period 2000–2009. Surface forcing was accomplished through the use of SST climatology derived from OISST data. SST values were obtained every 6 h through linear interpolation of the daily mean values.

Note that this approach does not capture realistic synoptic perturbations in West Africa, as the prescribed boundary conditions are based on climatological averages. However, previous studies have indicated that the model's eastern boundary (located at 50°E) is sufficiently far eastward to generate its own barotropic-baroclinic perturbations over the high reliefs of Sudan and the Ethiopian highlands that propagate westward as African easterly waves (Berry and Thorncroft 2005; Mekonnen et al. 2006; Kiladis et al. 2006). Therefore, in addition to the numerical noise, the model has the potential to produce its own physically-driven perturbations that contribute to the atmospheric circulation patterns in the region. As a result, the model potentially includes a considerable amount of noise caused by these perturbations. To assess the impact of this noise on precipitation over West Africa, we generate an ensemble of 11 different simulations with a 12-hour interval between each simulation. The first simulation in the ensemble is initiated on April 1 at 0000 UTC, followed by the second one on April 1 at 1200 UTC, the third one on April 2 at 0000 UTC, and so on: despite having identical boundary forcings, these simulations diverge significantly within a few days (not shown). This approach enables us to estimate the “natural” variance in precipitation resulting from numerical and physics noise in the simulated precipitation.

In the control ensemble, referred to as CTL, the observed climatological SST is prescribed across the entire Tropical Atlantic. Figure 1a, b shows the climatology for the months of July and August. Additionally, Fig. 1c, d displays the climatological difference between these two months, revealing a notable warming between 10°N and 25°N off the coast of

West Africa, as well as a cooling in the region of the cold tongue in the Gulf of Guinea during this period. The objective of the sensitivity experiments is to suppress this seasonal SST evolution: the model is forced with a similar climatological SST as in CTL, but with modifications applied to a specific region covering the entire Eastern Tropical Atlantic. This modified SST region is designed as a circular area for simplicity, with a buffer zone approximately 400 km wide to avoid sharp gradients (see Fig. 2):

- in the “Frozen North” (FzN) experiment, the SST warming is halted from June 10, while the cooling is allowed to continue (Fig. 2a). This results in a cold SST anomaly of up to  $-3^{\circ}\text{C}$  located northeast of the marine Intertropical Convergence Zone (ITCZ), off the coast of Senegal and Mauritania (Fig. 2b),
- in the “Frozen South” (FzS) experiment, the SST cooling is halted from June 10, while the warming is allowed to continue (Fig. 2c). This produces a warm SST anomaly of up to  $+3^{\circ}\text{C}$  in the Equatorial and Tropical South Atlantic (Fig. 2d).

In short, in these two experiments, we maintain a constant SST in the eastern Atlantic after June 10, resulting in warm or cold SST anomalies relative to the reference ensemble during July–August. The three ensembles, each consisting of 11 simulations (CTL, FzS, and FzN), are then averaged, and the differences between the experiments and CTL are examined to better understand the response of the atmospheric circulation and precipitation to these SST changes. Only the differences that show statistical significance at the 95% level (determined by a p-value of less than 0.05) with a Student's test are discussed in the following analysis.

### 2.3 Calculation of the humidity transport

In this study, the influence of changes in SST on humidity transport is investigated following the approach of Cadet and Nnoli (1987), Fontaine et al. (2003) and Meynadier et al. (2015). Humidity transport (hereafter HT) is calculated as follows (1):

$$Q = \frac{1}{T} \int_0^T -\frac{1}{g} \left( \int_{P_b}^{P_t} q V_h dp \right) dt \quad (1)$$

where  $g$  is the gravitational acceleration,  $q$  the specific humidity,  $V_h$  the horizontal wind,  $P_b$  and  $P_t$  the lower and upper limits of the vertical integration, and  $T$  the time average considered. Vertical integration is used for three distinct layers: the total troposphere (from the surface ( $P_s$ ) to 100 hPa), the lower troposphere ( $P_s$  to 850 hPa) and the upper troposphere (850 to 100 hPa).

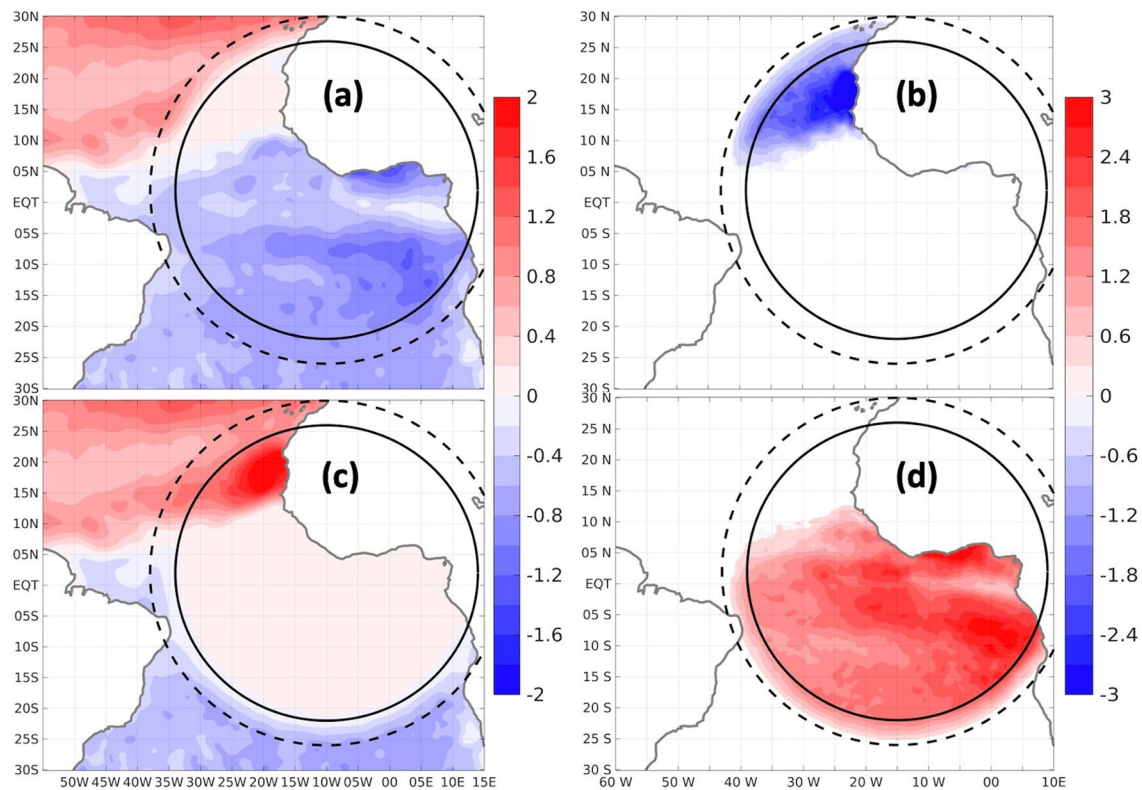


**Fig. 2** Spatial patterns of SST used as forcing in the FzN (a, b) and FzS (c, d) experiments. a and c the difference between August and July, b and d the difference between FzN and CTL in the July–August

average. The region where the SST modifications are fully applied is indicated by the plain black circle, and its buffer zone is marked by a dashed circle

### 3 Validation of the control experiment (CTL)

In general, regional and global models can exhibit differences due to the non-hydrostatic nature of global models, unlike regional models. Most coupled ocean–atmosphere General Circulation Models (GCMs) suffer from significant sea surface temperature (SST) biases in the tropical Atlantic and struggle to accurately represent the Atlantic Zonal Mode (Richter et al. 2014). However, the challenge is different for regional models, as different sets of parameterizations can produce very different simulations for the same model. This issue was studied in depth in Meynadier et al. (2015) for the WRF model, where numerous parameterizations were tested in order to optimize the representation of surface winds in the Gulf of Guinea, resulting in an improved climatological representation of the entire region, particularly precipitation. We have used the same parameterizations as them, and again we find a good comparison of July–August precipitation between WRF simulations and TRMM observations (Fig. 3a, b). Over the Atlantic Ocean, both models show maximum precipitation between around 5°N and 12°N over the ocean, and between 8°N and 15°N over the continent. The difference between the CTL ensemble mean and observations

in July–August (Fig. 3c) shows fairly small biases over the ocean, with only slight positive values around 10°N and negative values between 5°N and 10°N off the coast, indicating that the ITCZ is well represented but located slightly too far north in the CTL simulations (Fig. 3c).

On the continent, the model clearly overestimates precipitation. Quite large positive bias values (> 6–8 mm/d) are found in the position of the mean precipitation band (roughly between 8°N and 13°N): this excessive continental precipitation bias, associated with low surface wind speeds with the same set of parameterizations as us, is also commonly observed in many other WRF configurations (Meynadier et al. 2015): this problem could potentially come from high levels of soil moisture combined with higher shortwave radiative fluxes, leading to increased latent heat fluxes that help humidify the initially dry atmosphere over West Africa. That said, this bias is notably small compared to precipitation obtained with other regional atmospheric models (Gbode et al. 2019), such as the models used in the CMIP5 experiments (Richter et al. 2017), the Community Atmospheric Model version 4.0 (CAM4, Crespo et al. (2019)), or the GFDL climate model version 2.5 (CM2.5, Doi et al. (2012)). Precipitation in July–August is then fairly well represented by the model.

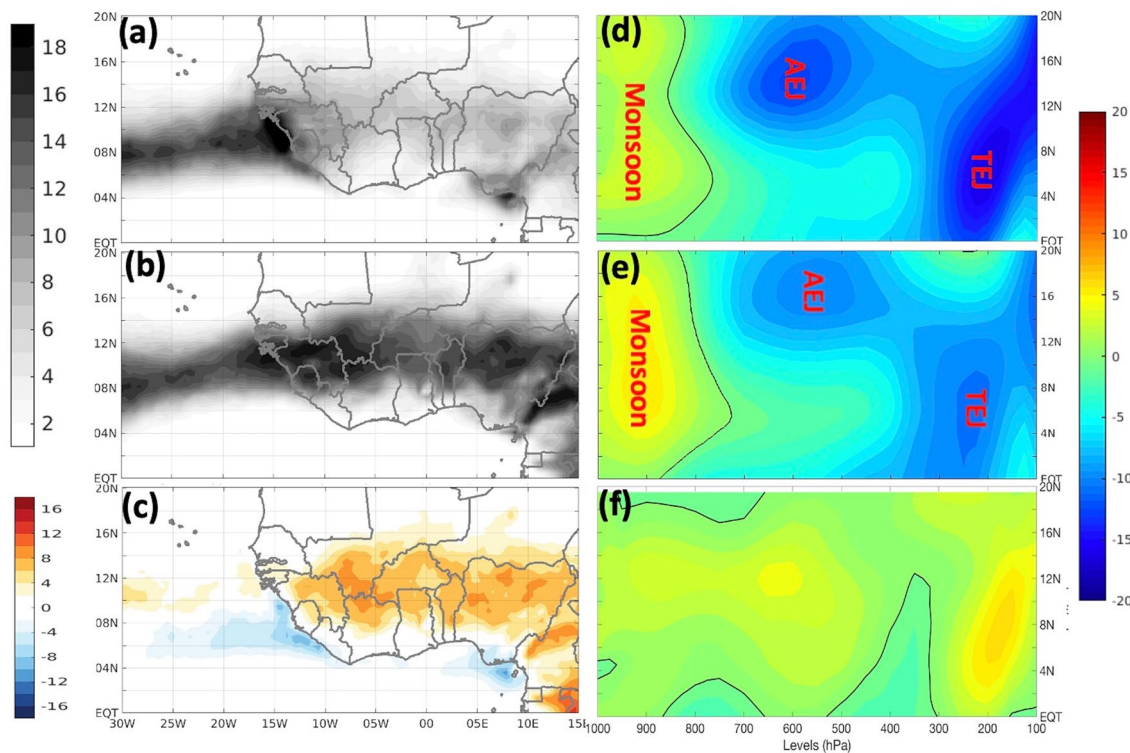


**Fig. 3** 2000–2009 July–August precipitation ( $\text{mm.d}^{-1}$ , left): TRMM observations (a) and CTL ensemble simulation (b). c shows the difference in CTL ensemble minus observations. Latitude–altitude diagram of zonal wind averaged in  $6^{\circ}\text{W}$ – $0^{\circ}\text{E}$  ( $\text{m.s}^{-1}$ , right): July–August

average in ERAI reanalyses (d) and in CTL ensemble simulation (e). d shows the difference CTL ensemble minus ERAI. The black contour in (f) delimits the zero value of zonal wind

In addition, a vertical meridional cross-section of the zonal wind in CTL is plotted in Fig. 3e and compared with the ERA interim reanalyses (Fig. 3d):

- the Tropical Easterly Jet around  $5^{\circ}\text{N}$  is slightly less intense in CTL (around  $10$ – $12$   $\text{m/s}$ , instead of around  $15$   $\text{m/s}$  in ERA interim) and is located slightly too low (its core is at  $250$  hPa compared with  $200$  hPa in ERA interim),
- the East African Jet (AEJ) is located slightly too far north and too high (its center is around  $15^{\circ}\text{N}$  at  $600$  hPa in ERA5, and around  $17^{\circ}\text{N}$  at  $550$  hPa in CTL),
- the monsoon flow is slightly more intense in CTL (up to  $7$   $\text{m/s}$  vs. less than  $5$   $\text{m/s}$  in CTL).

Apart from these few shortcomings, these dynamic elements, which are the main features of West African atmospheric circulation in boreal summer, are well represented in CTL. The chosen WRF configuration is therefore an appropriate tool for studying the seasonal migration of the tropical Atlantic ITCZ and the West African monsoon in boreal summer.

## 4 Response of the lower atmosphere to SST changes

We first study the impact of SST anomalies in the FzN and FzS experiments on sea level pressure (SLP) and surface winds. For these time scales (seasonal averages), the surface wind is the result of a balance between the pressure gradient, Coriolis forces, frictional forces, and an advection term that can be important in areas where the Trade Winds blow regularly (as with the Southeast-erlies in the Gulf of Guinea, see for example Meynadier et al. 2016, their figure 9). An SST gradient influences the surface wind via a local modification of the pressure gradient through hydrostatic adjustment (Lindzen and Nigam 1987): following this mechanism, a warm SST anomaly should therefore lead to an adjustment of pressure gradient forces towards its center, whereas a cold anomaly should lead to wind anomalies turned outwards.

This is what is actually observed in the FzN and FzS experiments: in FzN, the blocking of seasonal SST warming leads to a negative SST anomaly of up to  $-3^{\circ}\text{C}$  in



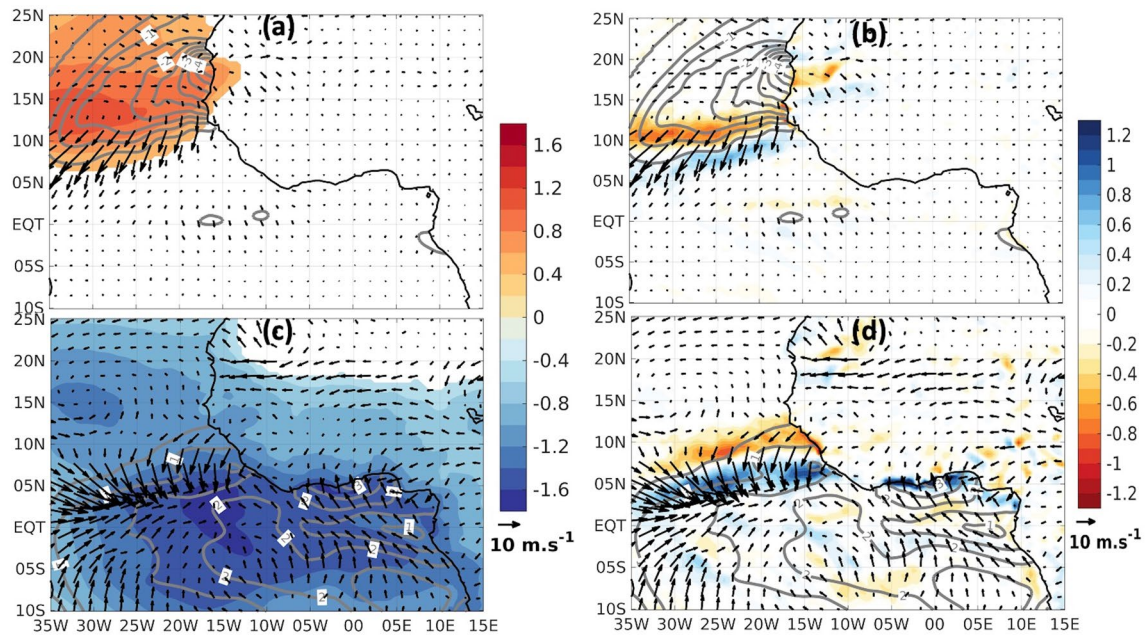


**Fig. 4** Differences in 2000–2009, July–August: Frozen North (FzN) minus CTL (**a**, **b**) and Frozen South (FzS) minus CTL (**c**, **d**). **a** and **c**: SLP anomalies (in hPa) as shading, **b** and **d**: surface wind convergence anomalies (in  $10^{-5} \text{ s}^{-1}$ ) as shading. The contours depict the SST

anomalies (in  $^{\circ}\text{C}$ ), and the vectors represent the 10 m-surface wind (in m/s). The SST anomalies (contours) are similar to those shown in Fig. 2b,d (shading)

the northeast tropical Atlantic region (hereinafter NETA, Fig. 2b). This cold SST anomaly (also shown in the grey contours of Fig. 4a, b) locally increases the SLP by +0.5 to over +1 hPa (Fig. 4a), creating a strong pressure gradient between around  $7^{\circ}\text{N}$  and  $13^{\circ}\text{N}$  leading to north/northeast surface wind anomalies (Fig. 4a, b). And in FzS, the warm SST anomaly in the ACT (Fig. 4c, d, grey contours) induces a decrease in SLP by more than  $-1 \text{ hPa}$  (Fig. 4c, shading), creating a strong front between the Equator and  $10^{\circ}\text{N}$  which generates northerly wind anomalies (Fig. 4c, d). Note that other surface wind anomalies than those discussed are also observed, but they are smaller and may not be significant.

In FzN, the wind anomalies are superimposed on the mean Trade Winds (Fig. 1b): they reflect an acceleration of the northeast Trade Winds and a deceleration of the southeast Trade Winds, resulting in a dipole of anomalies in surface wind divergence: positive (divergent) north of  $8^{\circ}\text{N}$ , and negative (convergent) further south (Fig. 4b, shading). The northward migration of the southeast Trade Winds (seen between July and August in Fig. 1d) is then counteracted by the cold SST anomaly: a weaker than normal NETA SST warming in boreal summer tends to oppose the northward migration of the ITCZ.

In FzS, the warmer-than-normal SST in ACT generates a local decrease in SLP, also from 0.5 to just over 1 hPa. Note that the warm SST anomaly in the ACT is much more geographically extensive than the cold SST anomaly in

NETA, so the region where it impacts SLP is also much larger. It weakens the strength of the meridional pressure gradient between the equator and  $10^{\circ}\text{N}$ , inducing a slowing of the southeasterly trade winds (Fig. 4c, d). As in FzN, there is a dipole of divergence anomalies (divergent / convergent) in the surface winds, but located slightly further south between around  $2^{\circ}\text{N}$  and  $10^{\circ}\text{N}$  (Fig. 4d, shading), and with an amplitude slightly greater than that due to the NETA SST anomaly. In the Gulf of Guinea, the warm SST anomaly strengthens southerly winds and increases coastal convergence on the Guinean coast, in agreement with Tanguy et al. (2022). It also weakens the ocean-continent pressure gradient, probably slowing southwesterly flows penetrating the continent and reducing zonal wind intensity in the western Sahel.

In short, the surface atmospheric response in the FzN and FzS experiments indicates that the seasonal warming in the NETA and cooling in the ACT both contribute to the northward migration of the ITCZ in July–August over the ocean. It is noteworthy that the warm anomaly in ACT sea surface temperatures appears to have the most significant impact, likely due to its larger spatial extent compared to the cold anomaly in NETA. Additionally, notable changes in surface winds are observed over the continent in both experiments. Given that these wind modifications affect humidity transport and subsequently precipitation, further analysis of this aspect is presented in the following section.



## 5 SST influence on humidity transport and precipitation

The average humidity transport (HT)  $Q$  during July–August is depicted for each layer in Fig. 5 as arrows, accompanied by its divergence,  $\nabla \cdot Q$ , represented by shadings.

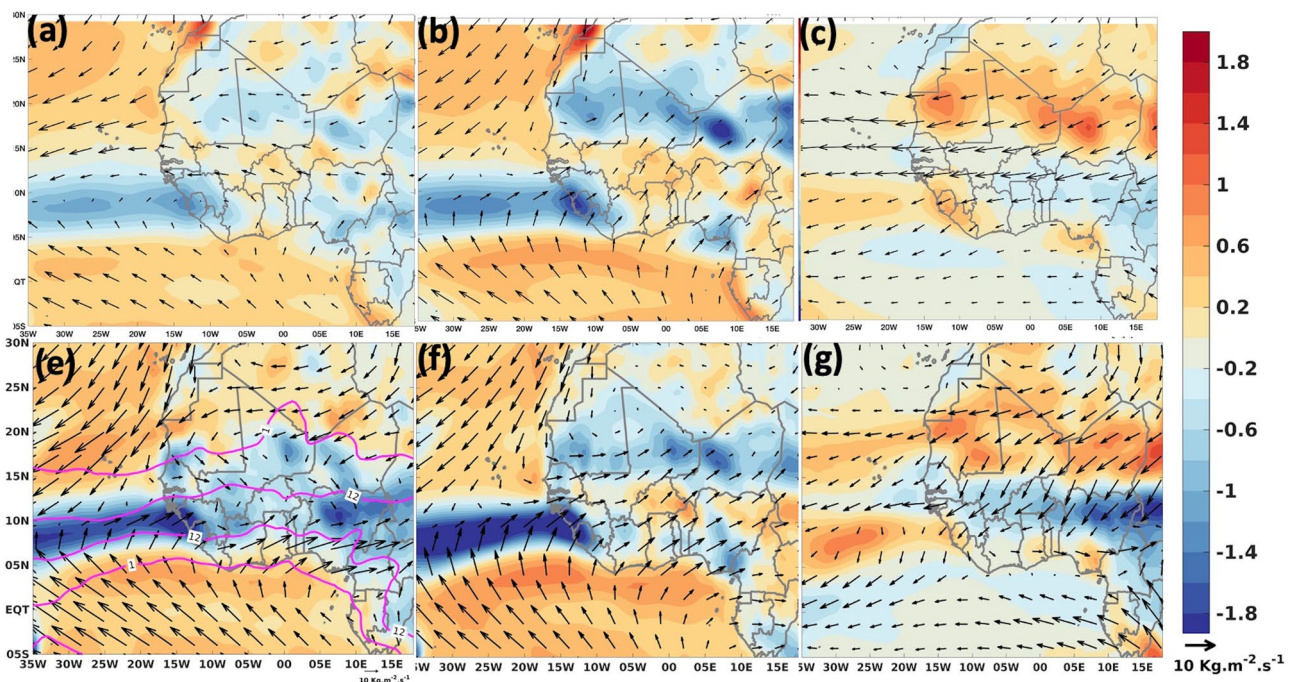
### Comparison between CTL simulation ensemble and ERA interim reanalyses

Figure 5 provides a reliable depiction of the spatial distribution of HT (arrows) and its divergence (shading) across the entire tropospheric column, as simulated by the WRF model (Fig. 5d–f), in comparison to the data provided by ERAI reanalyses (Fig. 5a–c). It is noticeable that the WRF model tends to overestimate HT and its convergence in the upper troposphere over the continent (Fig. 5f). This overestimation of HT convergence could potentially account for the higher rainfall values simulated by the WRF model (Fig. 3a, b).

Over the ocean, the HT is primarily concentrated in the lower troposphere, as evident when comparing Fig. 5a, e and b, f. The Trade winds strengthen as they approach the ITCZ, where the HT converges and subsequently diverges outside the ITCZ. A divergent HT is also observed with the southern monsoon flow in the Gulf of Guinea (Fig. 5b, f). Within the ITCZ, which spans approximately from 5°N

to 12°N, humidity increases due to the convergence of HT and is transported to the upper layers through convection and updrafts. As a result, the HT becomes slightly divergent in the upper layers (Fig. 5c, g). Notably, there is excellent agreement between the zonal band of convergent HT throughout the troposphere (depicted as blue regions) and the occurrence of heavy precipitation between 5°N and 12°N (shown as magenta contours in Fig. 5e).

Indeed, the fit between HT convergence and precipitation is generally good over the ocean: Weller et al. (2017) found that between 65% and 90% of precipitation is associated with long coherent lines of low-level convergence over the global oceans. The situation is less clear over land, where they were only able to associate 30–60% of low-level convergence with precipitation. Over southern West Africa in the lower troposphere, HT is mainly dominated by a south-western monsoon flow (Fig. 5b, e), with a strong westerly component close to the Atlantic Ocean consistent with the “West African westerly jet” investigated in previous studies (Pu and Cook 2012; Lélé and Leslie 2016). Two zonal bands of HT convergence are found: a moderate one along the Guinea coast between 5°N and 10°N, and a larger one further north between 15°N and 20°N (Fig. 5b, e). The latter, known as the Intertropical Front, is associated with no or little precipitation (“dry convection”, compare Fig. 5b, e and a, d). Instead, the precipitation maximum is localized between 8°N and 13°N, along the southern side of the AEJ



**Fig. 5** 2000–2009, July–August: HT ( $\text{Kg.m}^{-2}.\text{s}^{-1}$ , vectors) and HT divergence (shading,  $\text{s}^{-1}$ ) integrated from the surface to 100 hPa

(left), surface to 850 hPa (middle), and 850 to 100 hPa (right). **a–c** ERAI reanalyses. **d–f** CTL ensemble mean, with the CTL precipitation in magenta contours ( $\text{mm.day}^{-1}$ )

(Houze 2004; Dieng et al. 2014; Schumacher and Rasmusen 2020), where the HT is convergent in the upper troposphere (Fig. 5c, f). Note that the HT is oriented southward in WRF, but with a strong westward component consistent with the presence of the AEJ (between 500 and 700 hPa) and the TEJ (between 150 and 350 hPa, Fig. 3e).

#### *FzN minus CTL*

In FzN, over the ocean, the most significant change in the low troposphere is a northeastern HT anomaly between 5°N and 13°N, leading to a divergent/convergent dipole anomaly (Fig. 6b) induced by the northeasterly surface wind anomalies over the southern side of the cold SST anomaly (Fig. 4b) as discussed in the previous section. In the divergent HT anomaly between 9°N and 12°N, the precipitation is strongly damped between 8°N and 15°N (compare Figs. 6a and 5a; the difference between these figures is depicted in Fig. 8a). North of 15°N over the ocean, southwestern anomalies—albeit weak—in the lower troposphere indicate that less humidity is carried by the low-level Trade winds over the cold SST anomaly (Fig. 6b) which may contribute to the reduction of precipitation in the northern edge of the ITCZ.

Over the continent, no significant changes are detected in the lower troposphere (Fig. 6b). However, in the upper troposphere, a pronounced westward HT anomaly is observed between 10°N and 20°N (Fig. 6c). A latitude/altitude diagram, averaged over the 5°W–0°E longitude band, reveals that the core of this eastern HT anomaly is situated between

12°N and 17°N at an altitude of approximately 550–350 hPa (Fig. 7b). Figure 7a shows specific humidity (shading) and zonal velocity (contours) anomalies: while the specific humidity does not exhibit any significant anomaly, the zonal velocity displays a considerable negative anomaly ranging from  $-1$  to  $-3$  m/s precisely collocated with the HT anomaly. This indicates an acceleration of the African Easterly Jet (AEJ) just above its southern mean edge, between the average altitudes of the AEJ and the Tropical Easterly Jet (TEJ) (Fig. 3e). This zonal anomaly enhances the HT divergence between 13°N and 18°N (Fig. 6c), resulting in a decrease in precipitation between these latitudes, particularly west of 0°E, with a minimum of  $-3$  mm/day over Senegal (Fig. 8a). This decrease in precipitation could also be influenced by the reduction in HT inland due to a less intense West African Westerly Jet over the ocean. Divergent HT anomalies are also observed along the northeastern Guinea coast, east of Central Africa (Fig. 6b), coinciding with negative precipitation anomalies of up to  $-1.5$  mm/day (Fig. 8a).

#### *FzS minus CTL*

In FzS, over the continent, the main changes observed in the upper troposphere are a dipole in the HT divergence anomalies, negative (convergent) south of 12°N and positive (divergent) north of it (Fig. 6f). It relates to a strong westward acceleration of HT between 10°N and 20°N, which induces the northern HT divergence anomaly: the latter is consistent with a large decrease in precipitation east of 0°E

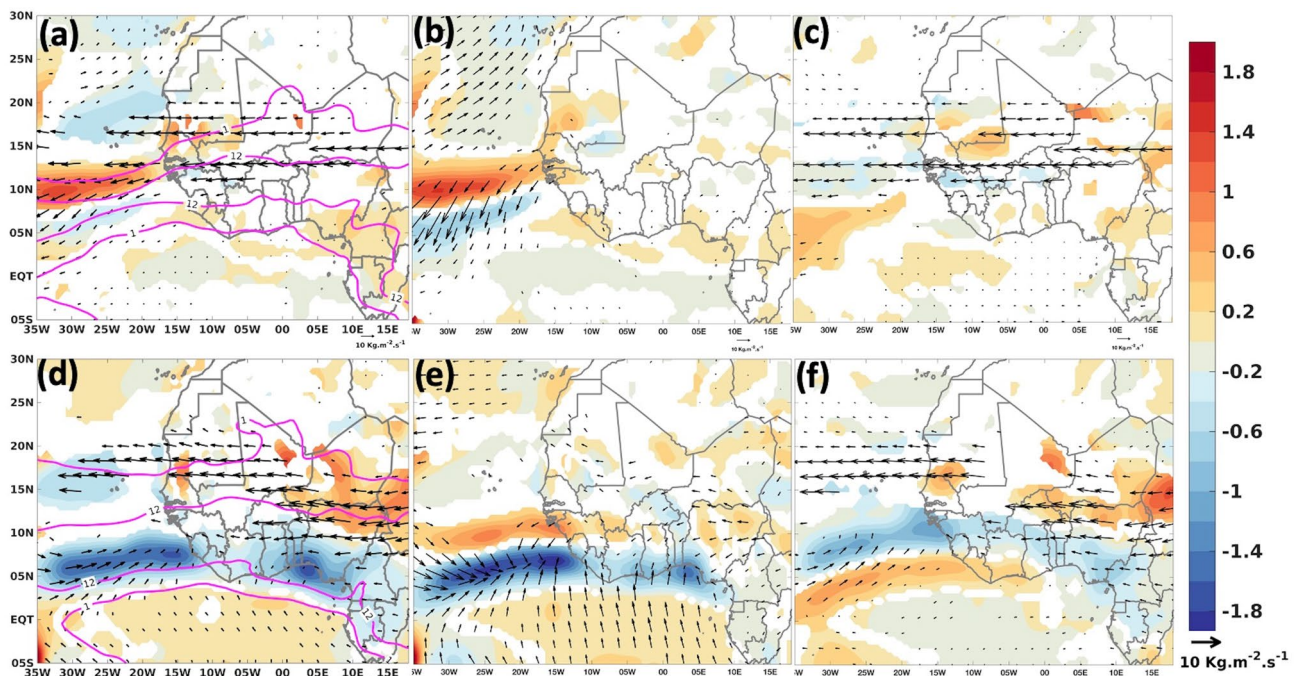


**Fig. 6** 2000–2009 July–August: HT ( $\text{Kg.m}^{-2}.\text{s}^{-1}$ , vectors) and HT divergence (shading,  $\text{s}^{-1}$ ) integrated from the surface to 100

hPa (left), surface to 850 hPa (middle), and 850 to 100 hPa (right). **a–c** ERAI product, **d–f** CTL ensemble mean, with precipitation in magenta contours ( $\text{mm.day}^{-1}$ )



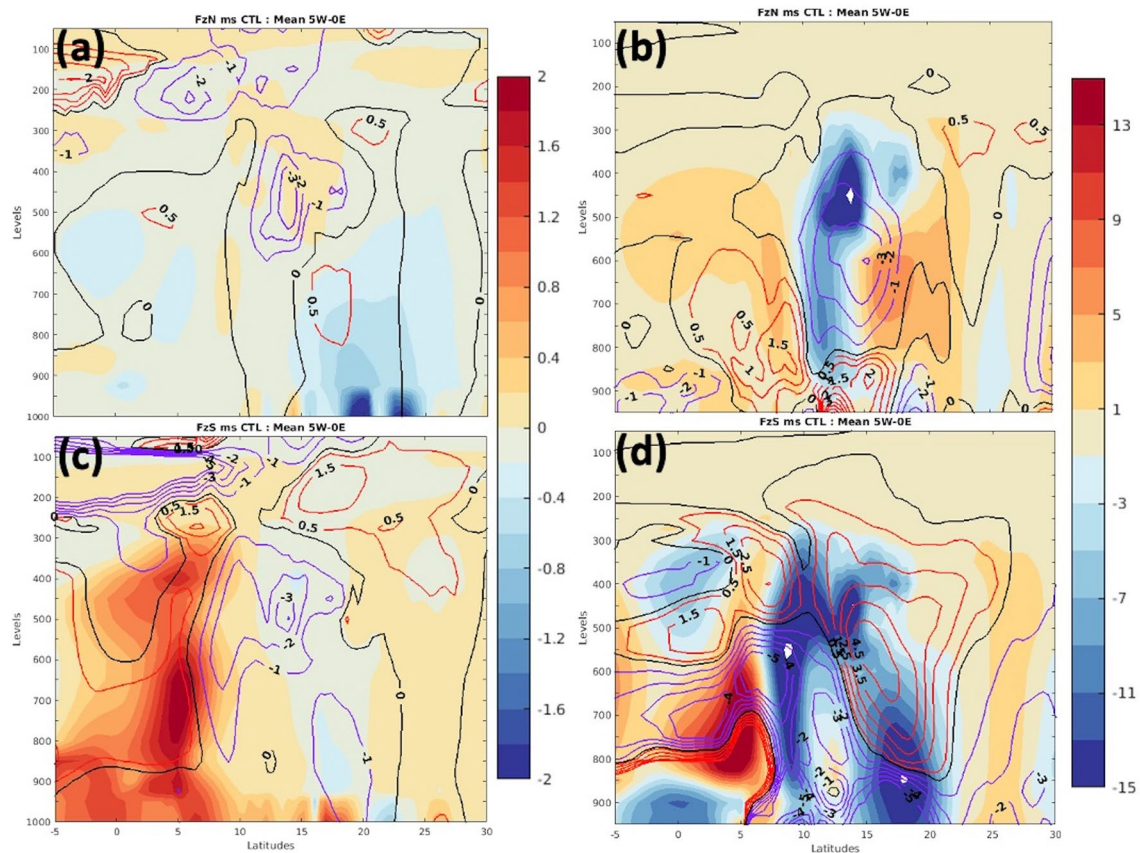


**Fig. 7** Latitude-altitude diagram, averaged in the 5°W–0°E region, depicting: **a, c** Specific humidity (shading,  $\times 10^{-3}$  Kg/Kg) and zonal wind (contours, intervals of 1 m/s). **b, d** Zonal HT (shading,  $\times 10^{-3}$  Kg.m $^{-2}$ .s $^{-1}$ ) and meridional HT (contours, intervals of 1 Kg.m $^{-2}$ .s $^{-1}$ ).

between 10°N and 15°N (Fig. 8b). As in FzN, the latitude/altitude diagram between 5°W and 0°E shows that the core of this westward HT anomaly corresponds to a negative (i.e., westward) zonal wind anomaly around 350–550 hPa, but is stronger than in FzN (up to -4 m/s) and extending further south while almost reaching the lower troposphere between 7°N and 11°N (Fig. 7c). In addition, the convergent HT anomaly south of 12°N extends to eastern Central Africa (Fig. 6f), superimposed to a strong band of increased convergence along the Guinea coast in the lower troposphere (Fig. 6e): the general intensification of the monsoon flow south of 5°N, due to the warm SST anomaly in the Gulf of Guinea, contributes to largely increase the coastal convergence in both the lower (at the coast) and upper (further downstream) troposphere, strongly favoring precipitation.

Over the ocean, there is a significant increase in convergence between 3°N and 8°N in the lower atmosphere (Fig. 6e), and this leads to a notable change in precipitation, characterized by a broadening of the rain band and intensified rainfall along its center (Fig. 6d, contours). It

The plots show the differences between FzN and CTL (**a, b**) and FzS and CTL (**c, d**). Blue contours represent negative values, red contours represent positive values, and the black contour indicates zero

results in a positive precipitation anomaly of over 7 mm/day observed between approximately 2°N and 10°N in the NETA (Fig. 8b).

#### Conclusion

A very good fit between positive (negative) HT divergence anomaly and negative (positive) precipitation anomaly is generally observed in both experiments, especially over the ocean. The HT divergence anomalies are expected to be created by the SST anomalies and to more easily quantify the effect of the latter on precipitation over the continent, and their relative contribution, already used to study the relative change in precipitation and temperature in climate models (Gaetani et al. 2020; Almazroui et al. 2020), is calculated as follows (2):

$$X_{exp} = \frac{P_{EXP} - P_{CTL}}{P_{CTL}} \quad (2)$$

where  $P_{EXP}$  is the precipitation in a given experiment (FzN or FzS) and  $P_{CTL}$  is the precipitation in the CTL ensemble.

The results are plotted in Fig. 8c,d:

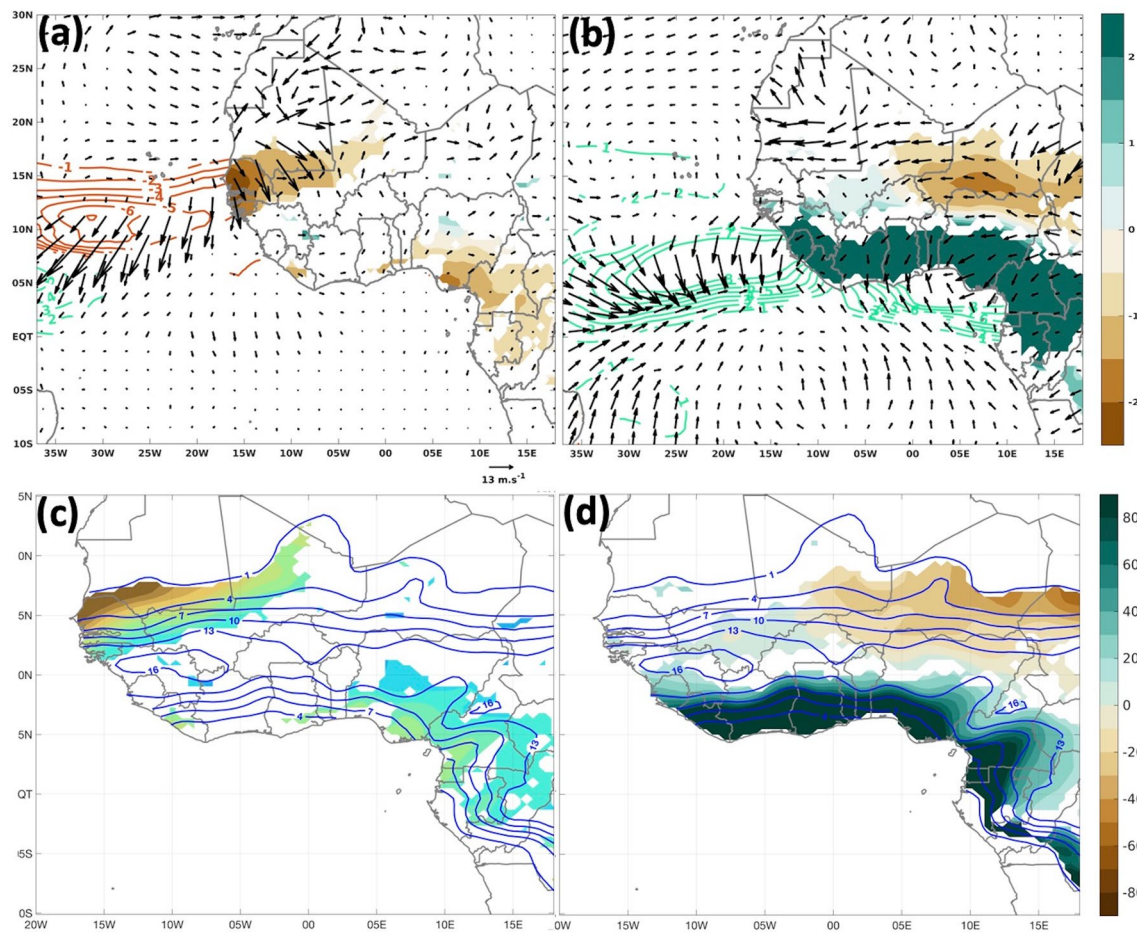


**Fig. 8** Top: differences between FzN and CTL (a) and FzS and CTL (b): total precipitation ( $\text{mm/day}$ ) and 10 m-surface wind ( $\text{m/s}$ , vectors). Precipitation over the continent is displayed in shading, while precipitation over the ocean is shown in contours (intervals of 1

$\text{mm/day}$ , with brown representing negative values and green representing positive values). Bottom: Relative change in precipitation (%) induced by FzN (c) and FzS (d). All differences are presented with a 95% significance level

- in FzN, precipitation is largely suppressed in the north-western Sahel region, specifically in northern Senegal, southern Mauritania, and Mali, where it is already relatively low on average (less than  $7 \text{ mm/day}$ , blue contours). Moreover, along the coasts of the Gulf of Guinea, there is a significant decrease in precipitation by up to 30–40% compared to the average (Fig. 8c),
- in FzS, precipitation almost doubles along the southern edge of the rainfall band, which includes the southern coast of West Africa and eastern Central Africa, where the July–August average is between 1 and  $10 \text{ mm/day}$  (Fig. 8c, blue contours). Additionally, there is a decrease in precipitation by up to 40–50% in the northeastern Sahel region, between  $12^\circ\text{N}$  and  $20^\circ\text{N}$ , east of  $0^\circ\text{E}$ .

An interesting insight arises from distinguishing between convective (thermodynamic) and non-convective (dynamic) precipitation. Figure 9b and d highlight that the increase in precipitation between  $8^\circ\text{N}$  and  $15^\circ\text{N}$  (ocean and continent)

in FzS is primarily of convective origin. However, a significant portion of this increase can be attributed to non-convective processes, driven by atmospheric dynamics and the convergence of near-surface HT. In the Gulf of Guinea, the increase in the monsoon flow leads to enhanced coastal convergence, resulting in a huge accumulation of humidity in the lower troposphere and favoring the deep atmospheric convection (Leduc-Leballeur et al. 2013). Furthermore, in the marine ITCZ, (Diakhaté et al. 2018) emphasized the important role of SST in influencing atmospheric dynamics and the convergence of HT, thereby impacting precipitation in the ITCZ.

The remaining precipitation anomalies are largely controlled by the divergence of HT. Specifically, over the ocean, the precipitation patterns, such as the drying effect observed north of the marine ITCZ in FzN, are influenced by the divergence of humidity transport in the lower troposphere. However, over the continent, the precipitation is more influenced by the divergence of HT in the upper troposphere. A



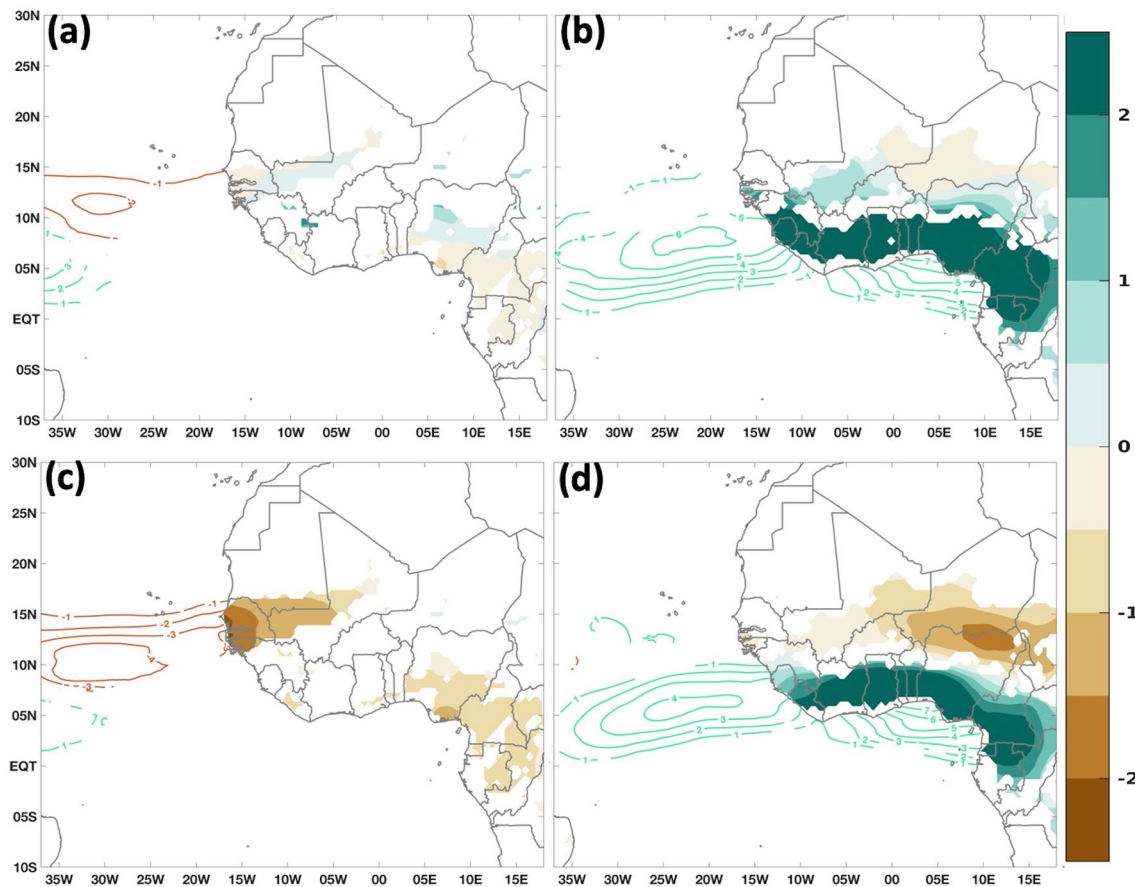


**Fig. 9** Same as in Figure 7a–b, but specifically for convective rain (a and b) and non-convective rain (c and d) in units of *mm/day*. The left panels depict the differences between FzN and CTL, while the right

panels show the differences between FzS and CTL. All differences are presented with a 95% significance level

positive anomaly of the latter is indeed observed in regions where there is a significant reduction in precipitation. In FzN, this is observed in the northwestern Sahel (Senegal, etc.) and the northeastern Gulf of Guinea / eastern Central Africa. Similarly, in FzS, a divergent HT anomaly in the upper troposphere is found in the northeastern Sahel, coinciding with reduced precipitation (Figs. 9, 10, 11).

## 6 Summary and conclusion

This study investigates the influence of SST anomalies in the eastern tropical Atlantic on the atmosphere and precipitation patterns over West Africa during the boreal summer. Ensemble simulations using the WRF model were conducted, comparing a control ensemble (CTL) with two experiments: Frozen North (FzN) and Frozen South (FzS), representing cold and warm SST anomalies, in the northeastern Tropical Atlantic (NETA) and in the Gulf of Guinea, respectively.

The simulations were evaluated against observed precipitation and ERA interim reanalyses, showing a reasonable

representation of the seasonal distribution of precipitation in July–August. The experiments involved altering the seasonal variation of SST within a wide circle covering the eastern Atlantic, starting from June 10. FzN resulted in a cold SST anomaly in the northeastern tropical Atlantic (NETA), while FzS produced a warm SST anomaly in the Equatorial and Southern Tropical Atlantic (ACT) region.

Over the ocean, FzN induced a local increase in surface pressure, accelerating the northeastern Trade winds and reducing the convergence of humidity transport in the northern ITCZ. In FzS, the warm SST anomaly weakened the meridional pressure gradient along the southern edge of the ITCZ, resulting in stronger convergence of humidity transport south of the ITCZ. Both experiments opposed the northward migration of the ITCZ over the ocean.

Over land, the SST anomalies had complex effects on precipitation patterns. In FzN, the cold SST anomaly dried the northwestern Sahel and the northeastern coasts of the Gulf of Guinea. In FzS, the warm SST anomaly increased precipitation just south of the marine ITCZ and along the coasts of the Gulf of Guinea, but dried the northeastern Sahel.

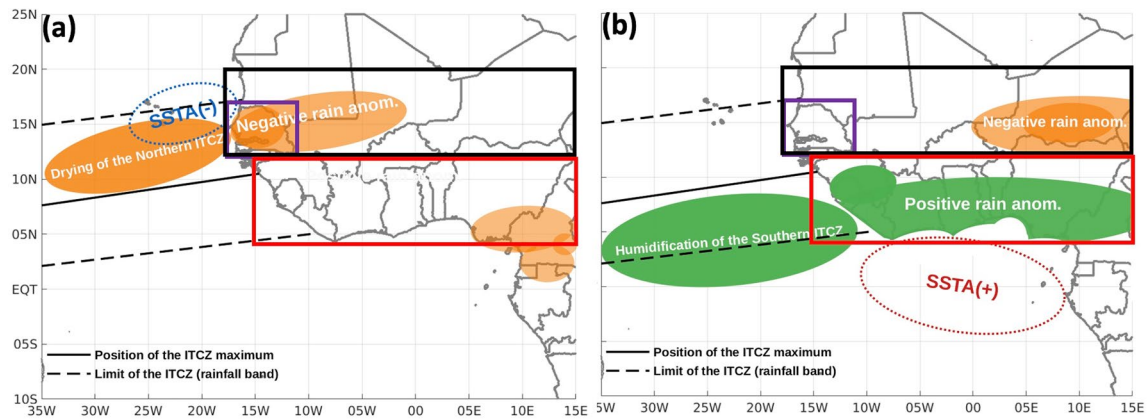


**Fig. 10** Impact of Eastern Tropical Atlantic SST on the marine ITCZ and West African rainfall during the boreal summer: **a** cold SST anomaly event in the Northeastern tropical Atlantic (FzN) = blue dashed oval. **b** Warm SST anomaly event in the Southeastern tropical Atlantic (FzS) = red dashed oval. The plain black line depicts the average position of the Atlantic ITCZ over the ocean, while the

dashed black line represents its northern and southern climatological limits. The increase in precipitation is represented by green patches, while the decrease in precipitation is represented by orange patches. The Sahelian, Guinean, and Senegalese regions are marked by black, red, and purple rectangles, respectively

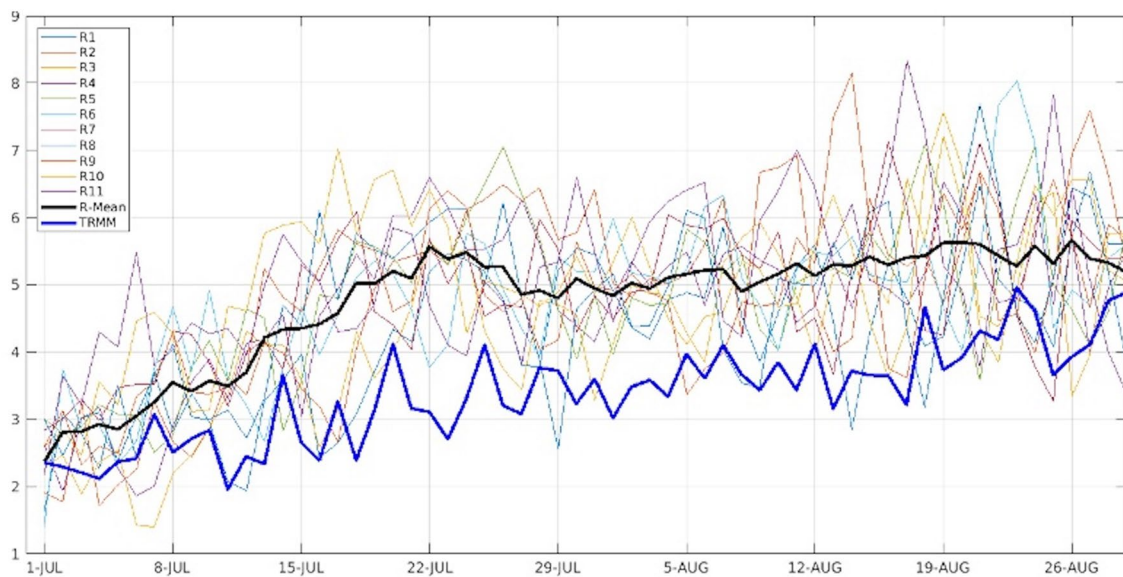


**Fig. 11** Rainfall time evolution, averaged over Sahel (12°–20°N and 20°W–20°E), in the WRF model runs (runs 1 to 11, represented by thin lines), their ensemble mean (thick black line), and the TRMM dataset (thick blue line)

Most of the precipitation anomalies observed in the experiments could be attributed to anomalies in humidity transport divergence. The SST anomalies also appeared to influence the zonal wind near the southern edge of the African Easterly Jet (AEJ). In the Sahel region, precipitation primarily originates from the Mesoscale Convective Systems (MCS) that form along the southern edge of the AEJ and its meanders (Parker et al., 2017). The northeastern Sahel precipitation anomaly in FzN could potentially be explained by changes in the horizontal vorticity field or baroclinicity,

favoring the formation of MCS. The mechanism linking the SST anomalies and zonal acceleration over the southern edge of the AEJ, which is known to be influenced by continental surface temperature and the meridional soil moisture gradient (Cook et al., 1999; Thiaw and Mo 2005; Talib et al., 2022), requires further investigation.

In FzS, the significant increase in coastal precipitation can be attributed to higher humidity in the troposphere compared to CTL, as a response to the warm SST anomaly in the ACT. Conversely, FzN exhibits a deficit of humidity in the same

latitude as the cold SST anomaly north of the ITCZ. These pronounced responses, particularly in FzS with its extended warm SST anomaly, were obtained with SST anomalies of up to 3°C, which are not very realistic considering interannual variability usually produces SST anomalies of only 0.5–1°C (Carton and Santorelli, 2008; Marin et al., 2009). However, the induced changes in precipitation are considerable, with FzS showing an increase of over 100% and both experiments resulting in a decrease of more than 50% in the northern Sahel. Further investigations are needed to more accurately quantify the effect of SST interannual variability on precipitation in the West African Monsoon.

In conclusion, this study provides insights into the impact of SST anomalies on atmospheric conditions and precipitation patterns, using simulations forced by mean climatology. The self-developed meteorological disturbances along the southern edge of the African tropical jets in the model simulations, without being influenced by large-scale synoptic situations at the model boundaries, may limit their realism. However, these disturbances exhibit some variability among simulations, despite identical boundary forcings, likely due to inherent numerical noise in the model. This natural variance within the model allows for an assessment of the robustness of SST-induced disturbances. This study serves as a necessary precursor to a more comprehensive investigation involving ensemble simulations conducted over multiple specific years, forcing the model with realistic large-scale synoptic situations. Such an approach will contribute to a better understanding of the mechanisms through which SST modifications disrupt precipitation patterns in West Africa.

**Author contributions** (applicable for submissions with multiple authors): All authors: Conceptualization; All authors: methodology; Dahirou Wane and Gaëlle de Coëtlogon: wrote the main manuscript; Dahirou Wane and Gaëlle de Coëtlogon: prepared all figures; Dahirou Wane, Gaëlle de Coëtlogon, Alban Lazar, and Malick Wade: prepared figures (1–2, 4–5, 7–8); Dahirou Wane, Gaëlle de Coëtlogon, and Alban Lazar: prepared Figure 9 and All authors reviewed the manuscript

**Funding** This work was supported by UK Research and Innovation as part of the Global Challenges Research Fund, grant number NE/P021077/1 (GCRF African SWIFT) and Centre d'Excellence Africain en Mathématique, Informatique et TIC (CEA-MITIC). The authors gratefully acknowledge financial support from the French Programme d'Investissements d'Avenir de l'Agence Nationale de la Recherche, through Contract ANR-17-MPGA-0015 (PRODUCT).

**Availability of data and materials** (a statement on how any datasets used can be accessed): All reanalyses and observational data sets are freely available. We thank the NOAA / NCDC for the Reynolds SST product, Copernicus Climate Data Service for the ERA5 data, and NASA GES DISC for the rainfall TRMM data. This work was granted access to the HPC resources of IDRIS under the allocation 0292 made by GENCI. We also thank GENCI for the availability of the ERAI forcing data sets, and server and storage of the WRF outputs simulations.

## Declarations

**Conflict of interest** (always applicable and includes interests of a financial or personal nature): none

**Ethical approval** (applicable for both human and/ or animal studies. Ethical committees, Internal Review Boards, and guidelines followed must be named. When applicable, additional headings with statements on consent to participate and consent to publish are also required): not applicable

**Open Access** This article is licensed under a Creative Commons Attribution 4.0 International License, which permits use, sharing, adaptation, distribution and reproduction in any medium or format, as long as you give appropriate credit to the original author(s) and the source, provide a link to the Creative Commons licence, and indicate if changes were made. The images or other third party material in this article are included in the article's Creative Commons licence, unless indicated otherwise in a credit line to the material. If material is not included in the article's Creative Commons licence and your intended use is not permitted by statutory regulation or exceeds the permitted use, you will need to obtain permission directly from the copyright holder. To view a copy of this licence, visit <http://creativecommons.org/licenses/by/4.0/>.

## References

- Almazroui M, Saeed F, Saeed S, Islam MN, Ismail M, Klutse NAB, Siddiqui MH (2020) Projected change in temperature and precipitation over Africa from cmip6. *Earth Syst Environ* 4(3):455–475
- Berry GJ, Thorncroft CD (2005) Case study of an intense African easterly wave. *Mon Wea Rev* 133:752–766
- Biasutti M, Battisti DS, Sarachik E (2004) Mechanisms controlling the annual cycle of precipitation in the tropical Atlantic sector in an atmospheric GCM. *J Clim* 17(24):4708–4723
- Brandt P, Caniaux G, Bourles B, Lazar A, Dengler M, Funk A, Hormann V, Giordani H, Marin F (2011) Equatorial upper-ocean dynamics and their interaction with the West African monsoon. *Atmos Sci Lett* 12(1):24–30
- Cadet D, Nnoli N (1987) Water vapour transport over Africa and the Atlantic Ocean during summer 1979. *Q J R Meteorol Soc* 113(476):581–602
- Carton JA, Santorelli A (2008) Global decadal upper-ocean heat content as viewed in nine analyses. *J Clim* 21(22):6015–6035
- Cook KH (1999) Generation of the African easterly jet and its role in determining West African precipitation. *J Clim* 12(5):1165–1184
- Crespo LR, Keenlyside N, Koseki S (2019) The role of sea surface temperature in the atmospheric seasonal cycle of the equatorial Atlantic. *Clim Dyn* 52(9):5927–5946
- de Coëtlogon G, Leduc-Leballeur M, Meynadier R, Bastin S, Diakhaté M, Eymard L, Giordani H, Janicot S, Lazar A (2014) Atmospheric response to sea-surface temperature in the eastern equatorial Atlantic at quasi-biweekly time-scales. *Q J R Meteorol Soc* 140(682):1700–1714
- de Coëtlogon Gd, Janicot S, Lazar A (2010) Intraseasonal variability of the ocean-atmosphere coupling in the gulf of guinea during boreal spring and summer. *Q J R Meteorol Soc* 136(S1):426–441
- Dee DP, Uppala SM, Simmons AJ, Berrisford P, Poli P, Kobayashi S, Andrae U, Balmaseda M, Balsamo G, Bauer DP et al (2011) The era-interim reanalysis: configuration and performance of the data assimilation system. *Q J R Meteorol Soc* 137(656):553–597

- Diakhaté M, Lazar A, de Coëtlogon G, Gaye AT (2018) Do SST gradients drive the monthly climatological surface wind convergence over the tropical Atlantic? *Int J Climatol* 38:e955–e965
- Dieng AL, Eymard L, Sall SM, Lazar A, Leduc-Leballeur M (2014) Analysis of strengthening and dissipating mesoscale convective systems propagating off the west African coast. *Mon Weather Rev* 142(12):4600–4623
- Doi T, Vecchi GA, Rosati AJ, Delworth TL (2012) Biases in the Atlantic ITCZ in seasonal-interannual variations for a coarse- and a high-resolution coupled climate model. *J Clim* 25(16):5494–5511
- Foltz GR, Brandt P, Richter I, Rodríguez-Fonseca B, Hernandez F, Dengler M, Rodrigues RR, Schmidt JO, Yu L, Lefèvre N et al (2019) The tropical Atlantic observing system. *Front Mar Sci* 6:206
- Fontaine B, Roucou P, Trzaska S (2003) Atmospheric water cycle and moisture fluxes in the west African monsoon: mean annual cycles and relationship using NCEP/NCAR reanalysis. *Geophys Res Lett* 30(3)
- Gaetani M, Janicot S, Vrac M, Famien AM, Sultan B (2020) Robust assessment of the time of emergence of precipitation change in west Africa. *Sci Rep* 10(1):1–10
- Gbode IE, Dudhia J, Ogunjobi KO, Ajayi VO (2019) Sensitivity of different physics schemes in the WRF model during a west African monsoon regime. *Theor Appl Climatol* 136(1):733–751
- Giannini A, Saravanan R, Chang P (2005) Dynamics of the boreal summer African monsoon in the nsipp1 atmospheric model. *Clim Dyn* 25(5):517–535
- Gill AE (1980) Some simple solutions for heat-induced tropical circulation. *Q J R Meteorol Soc* 106(449):447–462
- Gu G, Adler RF (2004) Seasonal evolution and variability associated with the west African monsoon system. *J Clim* 17(17):3364–3377
- Hastenrath S (2006) Circulation and teleconnection mechanisms of northeast Brazil droughts. *Prog Oceanogr* 70(2–4):407–415
- Hong S-Y, Lim J-OJ (2006) The WRF single-moment 6-class microphysics scheme (wsm6). *Asia-Pac J Atmos Sci* 42(2):129–151
- Hounsou-Gbo GA, Araujo M, Bourlès B, Veleda D, Servain J (2015) Tropical atlantic contributions to strong rainfall variability along the northeast brazilian coast. *Adv Meteorol* 2015
- Houze Jr RA (2004) Mesoscale convective systems. *Rev Geophys* 42(4)
- Huffman GJ, Bolvin DT, Nelkin EJ, Wolff DB, Adler RF, Gu G, Hong Y, Bowman KP, Stocker EF (2007) The TRMM multisatellite precipitation analysis (TMPA): Quasi-global, multiyear, combined-sensor precipitation estimates at fine scales. *J Hydrometeorol* 8(1):38–55
- Hulme M, Doherty R, Ngara T, New M, Lister D (2001) African climate change: 1900–2100. *Clim Res* 17(2):145–168
- Iacono MJ, Delamere JS, Mlawer EJ, Shephard MW, Clough SA, Collins WD (2008) Radiative forcing by long-lived greenhouse gases: Calculations with the AER radiative transfer models. *J Geophys Res Atmos* 113(D13)
- Janjić ZI (1994) The step-mountain eta coordinate model: further developments of the convection, viscous sublayer, and turbulence closure schemes. *Mon Weather Rev* 122(5):927–945
- Joly M, Voldoire A (2010) Role of the gulf of guinea in the inter-annual variability of the west African monsoon: what do we learn from cmip3 coupled simulations? *Int J Climatol* 30(12):1843–1856
- Kiladis GN, CDT, Hall NMJ (2006) Threedimensional structure and dynamics of African easterly waves. Part I: observations. *J Atmos Sci* 63:2212–2230
- Leduc-Leballeur M, de Coëtlogon G, Eymard L (2013) Air-sea interaction in the gulf of guinea at intraseasonal time-scales: wind bursts and coastal precipitation in boreal spring. *Q J R Meteorol Soc* 139(671):387–400
- Lélé MI, Leslie LM (2016) Intraseasonal variability of low-level moisture transport over West Africa. *Clim Dyn* 47(11):3575–3591
- Li T, Philander S (1997) On the seasonal cycle of the equatorial Atlantic ocean. *J Clim* 10(4):813–817
- Lin B, Wielicki BA, Minnis P, Chambers L, Xu K-M, Hu Y, Fan A (2006) The effect of environmental conditions on tropical deep convective systems observed from the TRMM satellite. *J Clim* 19(22):5745–5761
- Lindzen RS, Nigam S (1987) On the role of sea surface temperature gradients in forcing low-level winds and convergence in the tropics. *J Atmos Sci* 44(17):2418–2436
- Marin F, Caniaux G, Giordani H, Bourlès B, Gouriou Y, Key E (2009) Why were sea surface temperatures so different in the eastern equatorial Atlantic in June 2005 and 2006? *J Phys Oceanography* 39(6):1416–1431
- Mekonnen A, CDT, Aiyer A (2006) Analysis of convection and its association with African easterly waves. *J Clim* 19:5405–5421
- Meynadier R, de Coëtlogon G, Bastin S, Eymard L, Janicot S (2015) Sensitivity testing of WRF parameterizations on air-sea interaction and its impact on water cycle in the gulf of guinea. *Q J R Meteorol Soc* 141(690):1804–1820
- Meynadier R, de Coëtlogon G, Leduc-Leballeur M, Eymard L, Janicot S (2016) Seasonal influence of the sea surface temperature on the low atmospheric circulation and precipitation in the eastern equatorial Atlantic. *Clim Dyn* 47(3):1127–1142
- Mitchell TP, Wallace JM (1992) The annual cycle in equatorial convection and sea surface temperature. *J Clim* 5(10):1140–1156
- Okumura Y, Xie S-P (2004) Interaction of the Atlantic equatorial cold tongue and the African monsoon. *J Clim* 17(18):3589–3602
- Parker DJ, Kassimou A, Orji BN, Osika DP, Hamza I, Diop-Kane M, Fink A, Galvin JPM, Guichard F, Lamprey BL, Hamidou H, van der Linden R, Redl R, Lebel T, Tubbs C (2017) Local weather. In: Parker DJ, Diop-Kane M (eds) *Meteorology of tropical West Africa: the forecasters handbook*. Wiley, Chichester, UK, pp 130–174
- Pu B, Cook KH (2012) Role of the west African westerly jet in sahel rainfall variations. *J Clim* 25(8):2880–2896
- Reynolds RW, Smith TM, Liu C, Chelton DB, Casey KS, Schlax MG (2007) Daily high-resolution-blended analyses for sea surface temperature. *J Clim* 20(22):5473–5496
- Richter I, Xie S-P, Behera SK, Doi T, Masumoto Y (2014) Equatorial Atlantic variability and its relation to mean state biases in CMIP5. *Clim Dyn* 42:171–188
- Richter I, Xie S-P, Morioka Y, Doi T, Taguchi B, Behera S (2017) Phase locking of equatorial Atlantic variability through the seasonal migration of the ITCZ. *Clim Dyn* 48(11):3615–3629
- Rugg A, Foltz GR, Perez RC (2016) Role of mixed layer dynamics in tropical North Atlantic interannual sea surface temperature variability. *J Clim* 29(22):8083–8101
- Schumacher RS, Rasmussen KL (2020) The formation, character and changing nature of mesoscale convective systems. *Nat Rev Earth Environ* 1(6):300–314
- Shamarock WC, Klemp JB, Dudhia J, Gill DO, Barker DM, Wang W, Powers JG (2008) A description of the advanced research wrf version 3. NCAR technical note-475+ str
- Steinig S, Harlaß J, Park W, Latif M (2018) Sahel rainfall strength and onset improvements due to more realistic Atlantic cold tongue development in a climate model. *Sci Rep* 8(1):2569
- Sultan B, Janicot S (2000) Abrupt shift of the ITCZ over West Africa and intra-seasonal variability. *Geophys Res Lett* 27(20):3353–3356
- Sultan B, Janicot S (2003) The west African monsoon dynamics. Part II: The “preonset” and “onset” of the summer monsoon. *J Clim* 16(21):3407–3427



- Talib J, Taylor CM, Klein C, Harris BL, Anderson SR, Semeena VS (2022) The sensitivity of the West African monsoon circulation to intraseasonal soil moisture feedbacks. *Q J R Meteorol Soc.* <https://doi.org/10.1002/qj.4274>
- Tanguy M, de Coëtlogon G, Eymard L (2022) Sea surface temperature impact on diurnal cycle and seasonal evolution of the guinea coast rainfall in boreal spring and summer. *Monthly Weather Rev*
- Thiaw WM, Mo KC (2005) Impact of sea surface temperature and soil moisture on seasonal rainfall prediction over the Sahel. *J Clim* 18(24):5330–5343
- Thorncroft CD, Nguyen H, Zhang C, Peyrillé P (2011) Annual cycle of the West African monsoon: regional circulations and associated water vapour transport. *Q J R Meteorol Soc* 137(654):129–147
- Tomaziello ACN, Carvalho LM, Gandu AW (2016) Intraseasonal variability of the Atlantic intertropical convergence zone during austral summer and winter. *Clim Dyn* 47(5):1717–1733
- Vizy EK, Cook KH (2001) Mechanisms by which gulf of guinea and eastern North Atlantic sea surface temperature anomalies can influence african rainfall. *J Clim* 14(5):795–821
- Wahl S, Latif M, Park W, Keenlyside N (2011) On the tropical Atlantic SST warm bias in the Kiel climate model. *Clim Dyn* 36:891–906
- Waliser DE, Graham NE (1993) Convective cloud systems and warm-pool sea surface temperatures: coupled interactions and self-regulation. *J Geophys Res Atmos* 98(D7):12881–12893
- Wane D, Lazar A, Wade M, Gaye AT (2021) A climatological study of the mechanisms controlling the seasonal meridional migration of the Atlantic warm pool in an OGCM. *Atmosphere* 12(1224)
- Weller E, Shelton K, Reeder MJ, Jakob C (2017) Precipitation associated with convergence lines. *J Clim* 30(9):3169–3183

**Publisher's Note** Springer Nature remains neutral with regard to jurisdictional claims in published maps and institutional affiliations.